Energy, Volume 176, 1 June 2019, pp. 235-248
DOI: 10.1016/j.energy.2019.03.187

Experimental Investigation of Gas Turbine Compressor Water Injection for NO_x Emission Reductions

David Alejandro Block Novelo, Uyioghosa Igie*, Vinod Prakash, Artur Szymański

School of Aerospace Transport and Manufacturing, Cranfield University, Cranfield, UK

*u.igie@cranfield.ac.uk

Abstract

The global rising demand for civil air travel shows good prospects for the industry, however, this growth is inevitably matched with higher levels of emissions and fuel consumption. In this study, demineralised water injection is presented as an alternative to reduce NO_x emissions and enhance engine performance. The experimental study firstly presents the droplet size characterisation of a spray nozzle. This is done for varied injection pressure, water temperature and at varied axial and radial locations using an impaction pin nozzle. The single-shaft *Artouste* engine is used in conducting the compressor water injection test with water-to-air ratios of 0.5, 1 and 2%. The water droplet diameter, engine gas path and exhaust emissions are all monitored in real time. For the engine tests, droplets are measured at the spraying point and correlations are used to account for the droplet size at the inlet of the compressor due to measurement difficulties in this region. The test showed a reduction in compressor discharge temperature by up to 34 K and a NO_x decrease by 25%. Nevertheless, the higher reductions in NO_x at higher water-to-air ratios are attributed to a predominant cooling in the combustor because of unevaporated water in the compressor. At 0.5% water-to-air ratio, the drop in NO_x is mainly due to compressor cooling and signified by the only case in which the fuel-to-air ratio reduces. The study presents evidence of the combined effects of compressor and combustor water ingestion. The CO is seen to increase significantly and associated with reduced combustor efficiency.

Keywords: water injection, engine experiment, compressor, combustor, NO_x

1- Introduction

There are more aircraft flying today than ever before and civil air transportation is still expected to double within the next 14 years [1]. The promise of more accessible air travel has come with increasing concern about the effects of jet-engine pollutants at ground level and during flight. The increase in aircraft fleet has led to aviation-borne Nitrogen Oxide (NO_x) emissions doubling between 1990 and 2014, while Carbon Dioxide (CO_2) emissions increased by 80% [2]. Currently, only ground-level emissions (considered below 3,000 ft.) are regulated, by limiting the maximum levels of pollutants that aircraft produce during take-off, climb, approach and idle. The regulated emissions are NO_x, Carbon Monoxide (CO), and unburned hydrocarbons (UBH) that are controlled through the International Civil Aviation Organization (ICAO). Airports have also attempted to mitigate this problem by charging airliner operators an environmental fee, based on the mass of pollutants that aircraft engines produce. In the pursuit of meeting these regulations, engine manufacturers and operators have implemented programs to reduce exhaust emissions and fuel burn. The most common approaches for ground-level fuel reductions are limiting the on-time of the engines. These are: by deploying single engine taxing, towing vehicle- taxing, queue management or by limiting the use of the Auxiliary Power Unit (APU) [3–5]. Nitrogen Oxide emissions formed in the combustion chamber at high temperatures are especially relevant during take-off when the turbine inlet temperature (TIT) peaks. These emissions are harder to control as they depend on the engine pressure ratio and temperature (which has been rising to attain superior fuel efficiency) and on the residence time of the

Published by Elsevier. This is the Author Accepted Manuscript issued with: Creative Commons Attribution Non-Commercial No Derivatives License (CC:BY:NC:ND 4.0).
The final published version (version of record) is available online at DOI:10.1016/j.energy.2019.03.187. Please refer to any applicable publisher terms of use.

gas in the primary combustion zone. For this reason, research has been conducted in redesigning the combustion chamber to cool down the operation, burn the fuel-air mixture in a lean way, or modify the gas residence time [6]. Fuel efficiency and emissions reductions have also been achieved through the improvements in the design or modification of other main engine components like the compressor and turbine. Significant advancements have been achieved in this area by deploying multiple spools, employing variable stators, implementing better blade profiles and advanced cooling, all of which have resulted in reaching peak component efficiency and on expanding the range of safe operations. Despite this, the maximum thermal efficiency of the cycle is about 41% and one of the major sources of entropy generation according to Grönstedt et al. [7] is the core exhaust loss. The loss is associated with the thermal energy lost to the surroundings and in the exhaust flow of the engine. In stationary gas turbines, this heat can be recovered through steam generation to drive a steam turbine to achieve up to 60% plant efficiency. A promising alternative that could tackle both (emissions and core exhaust losses) when constrained to just the engine as in the case of jet engines is through intercooling the compressor. This will reduce the cycle temperature (and thus wasted heat energy at the exit) for the same thrust settings, allowing for similar or greater compressor exit pressures accompanied by lower exit temperatures throughout the engine and the exhaust. The focus of this study is on injecting atomized water into the compressor of the gas turbine to reduce NO_x emissions and improve the performance of the engine. The small size of the engine used, and hence operating temperatures and pressures have brought about an added opportunity to also examine the effects of combustor water injection that is known to be more promising at reducing NO_x emissions.

Compressor water injection: Previous analysis based on analytical or numerical methods predict that the core air mass flow can be cooled by 12% [8,9] and as a consequence reduce NO_x emissions by up to 50% [9–12]. To the knowledge of the authors, only a few experimental studies have been performed in this area. Utamura et al. [13,14] show the promise in reducing the compressor exit temperature and specific compressor work. The study predicts up to 10% increase in power output with only 1% water-to-air ratio. The study is compared to analytical predictions. Jolly [15] presents very similar figures as the previous study and reports changes in temperature (-7.4%) and pressure (+3.2%) of a 35 MW industrial installation under inlet fogging conditions (1% of the air flow). These engine-based studies show the performance changes due to compressor water injection but do not include droplet size distribution analysis and the corresponding exhaust emissions. Other experimental studies involve the work of Roumeliotis and Mathioudakis [16] for a single stage compressor which highlights the aerodynamic implications of water injection. The study shows an increase in the amount of compressor power consumed for the same throttle position. No significant changes in the flow pattern, stall margin or pressure rise were observed for up to 2% water-to-air ratio investigated. The study focuses on the stand-alone compressor component and does not provide details about the droplet size distribution. Schnitzler et al. [17] extended the problem to a multistage stand-alone compressor. The work includes droplet measurements and concludes that injecting water into the compressor can improve the efficiency of the turbo component. A recent experimental study also on a stand-alone multi-stage compressor was also presented by Munari et al [18]. The study examines an axial-centrifugal compressor operating under steady state, surge and rotating stall conditions. The investigation concludes that water injection has no considerable negative effect on the surge margin under the conditions examined.

***Combustor water injection*:** Bahr and Lyon [19] experimentally investigated the implications of water injection into LM2500 and LM5000 land-based gas turbine combustors. The study shows that injecting water directly in the combustor can reduce NO_x emissions by up to 90%. The engine with the lowest compression ratio (LM2500) was penalized with a sharp increase in CO emissions due to a reduction in combustion efficiency. Although combustion water injection has a great promise in reducing NO_x

emissions, it does not provide the advantage of reduced compressor work and is often associated with an increase in Specific Fuel Consumption (SFC) [13]. Walsh and Fletcher [20] indicate that a water-to-fuel ratio of 1 could increase the SFC of an engine by 6-8% while producing a three-fold increase in CO emissions. Shahpouri and Houshfar [21] present a numerical model of a conventional combustor operating with humid air (only water vapour) and water injection. The study also noticed a rise in CO with direct water injection, but a decrease with humid air. In both cases, the NO_x emissions were reduced, though this reduction was more significant with direct water injection. The developments of Dry Low Emission combustors that deploys lean premixed combustion has brought about a significant reduction in NO_x emissions for power generation applications. However, for jet engines, diffusion combustors produce higher levels of NO_x but generally more stable and efficient combustion at wider operating envelopes. Daggett [11,22] reports the last application of wet combustion for the early 747-100 and 747-200 using a Pratt & Whitney JT9D-3AW and 7AW series engines. Problems related to the poor temperature distribution in the high-pressure turbine and hotspots are indicated by the author. The study also indicates that this problem was resolved in the industrial application. The referred study also provides evidence of the impact of combustor water injection at different water-to-fuel ratios, through simulations. At 0.5 ratio for constant thrust operation, there is a 50% reduction in NO_x emission, 80 K drop in TIT and about 2% increase in SFC. Wilkes [23] shows the case of increased power (3.3% rise) at the same water-to-fuel ratios. The NO_x reduction is shown to be about 50% and around 1.5% decrease in thermal efficiency (that is an increase in SFC). Blazowaki [24] shows that for the same water-to-air ratio, the combustor water injection is more promising for NO_x reduction, thereby inferring relatively less water required for the same decrease. Despite the advantages, as would be observed in the present study, the negative effects on increased fuel burn, CO/ hydrocarbon emissions, and sooth is still to be addressed.

Droplet Characterisation: Extensive experimental work on the science of water misting or water injection has been conducted by Chaker et al. [25–28]. Most of the published work is based on droplet dynamics and the methodology for measuring fogging sprays. These studies do not include engine performance analysis and are entirely based on inlet fogging for industrial gas turbines. Droplet measurements were performed using fogging nozzles with a diffraction laser tracking the spray plume axially and transversally, and this approach forms the basis of the present work. Savic et al. [29] studied nozzle sprays for different flow velocities and considering different nozzle orientation (in line with the flow, cross flow and opposite to the flow direction). The investigation provides valuable information about nozzle and droplet interaction. The influence of ambient conditions (temperature and relative humidity) as well as water temperature, measuring position and injection pressure on droplet size was also studied and presented by Chaker et al. [26]. The study concludes that the environmental conditions have a minor effect compared to the injecting properties (when studying droplet decay and temperature reductions of the surrounding air).

The present investigation corroborates some of the results obtained in Refs. [25,28,29] for single impaction pin nozzle, and subsequently applies the fogging nozzles to the inlet of a gas turbine. This nozzle type was chosen over other types of nozzles (flat spray and hollow cone) as they are characterised by smaller droplet sizes without compromising the water flow delivery, as noted by Ref. [25]. A parametric analysis is presented considering varying injection pressures, identical nozzles and varied distances from the nozzle exit: axially and radially. The droplets were measured by means of laser diffraction, using a Malvern Spraytec laser equipment. For the engine test, the nozzle manifold was installed in front of the engine bellmouth. Due to the difficulty in measuring the droplet size at the entrance of the compressor, empirical correlations from Ref. [30] were used to account for the droplet size between the measuring station and the compressor intake. The results presented here bring together the estimated droplet size at the intake of

the engine with the performance and emissions changes during water injection. Though the water injection takes place in the compressor section, the study brings together the combined effects of evaporation in the compressor and combustor, as a result of incomplete vaporisation of the former. This is directly due to the small size of the engine that is associated with lower operating temperatures and pressures. The achievement of this study, therefore, is to provide evidence for the implications of injecting water into a gas turbine, with the combined water effects from both components, in an area dominated by analytical and numerical studies which do not often capture some of the practicalities of deploying this technology. The change in gas path performance (temperatures, pressures and flows), as well as the exhaust emissions and the water droplet size, are monitored in this study by means of experimental tests performed on a single-spool engine.

2- Methods: Droplet Measurement in still air

2.1 Experimental set-up

A nozzle spray consists of a distribution of particles or droplets of different sizes. The interaction between the droplets (break-up, coalesce, bounce) makes it impossible to produce a homogenous droplet size composition. For this reason, when measuring a spraying plume at a given location, a number that represents the droplet size distribution is used rather than the actual particle size (explained subsequently). In this study, the instrument used to measure the droplets size is light diffraction Helium-Neon Laser (wavelength: 632.9 nm, power <5mw) capable of measuring particles from 0.1 to 2000μm. The laser emits a 10 mm diameter beam, which is scattered by the particles. This scattered light is collected into an array of detectors located on the receiver lens as depicted in Figure 1. The angle of the light diffraction is inversely proportional to the droplet size. As such, the laser equipment measures the angle at which the light is diffracted and not the droplet size directly. This instrument subsequently applies Fraunhofer approximation and Mie theory to translate the scattering pattern into particle size distributions, on the basis that each droplet will distribute the light at a specific angle depending on its size [31].

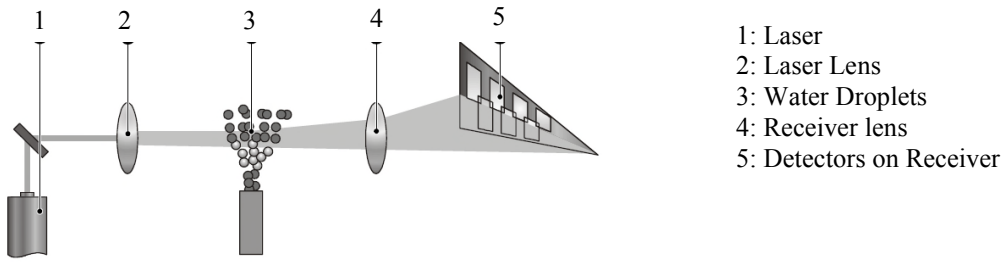

Figure 1 Laser scattering mechanism [31]

The presented method is well established for measuring droplet sprays and it has been previously applied in Refs. [25,27,29]. It also complies with the ASME standard for spray measurement [32] and according to the manufacturer, has a repeatability in measurement and an accuracy better than +/- 1% [31]. The numbers used to represent the sprays are the Sauter Mean Diameter (SMD) also referred to as D_{32}, and the Dv_{XX}, where XX can take the value of 10, 50 or 90. The Dv_{90}, for example, means that 90% of the volume of the spray is distributed in droplets of the specified diameter or smaller. The SMD, on the other hand, is a diameter that has the same volume-to-surface-area ratio as the average volume-to-surface-area ratio of all the droplets in the spray. This diameter is of high relevance for evaporative cooling applications because it expresses how much surface area of water is exposed to the air. The SMD values tend to be smaller than the Dv_{90}, since the Dv_{90} is an expression of the largest particle size present in the spray, while

the SMD refers to a representative diameter. Further details of the other diameters used to characterize the size distribution of a spray can be found in Ref.[33]. For this analysis, the spray was characterized by the Dv_{90} and SMD parameters. These values are a time-average of each measurement at each position and at the specified operating pressure. The time considered for each measurement was about 2 minutes and the droplet size is based on the following parameters:

- Operating Pressure (69 and138 bar)
- Nozzle (multiple identical impaction nozzles were tested)
- Water Temperature (288- 323K)
- Water type (demineralized and tap water)
- Axial positions from the nozzle tip (50 – 250 mm)
- Radial positions for a given axial location from the nozzle tip

The 138 bar operating pressure produces smaller droplet size distribution as seen subsequently and hence implemented in the engine analysis. The experimental setup for the droplet study consists of 4 units as indicated in Figure 2. In the figure, number 1 is the water injection skid consisting of a tank, a water pump, an electric motor and a pressure control valve. Number 2 refers to the impaction pin nozzle also shown in Fig. 3. The laser unit used to monitor the droplet diameter is labelled as 3. Droplet size measurements were taken at different positions along and across the plume. For these positions to be consistent, a 3-directional Parker-Hannifin® daedal positioning mounting was used. This mechanism labelled in Figure 2as 4, has a readability of 0.1 mm and a straight-line accuracy of 0.01%.

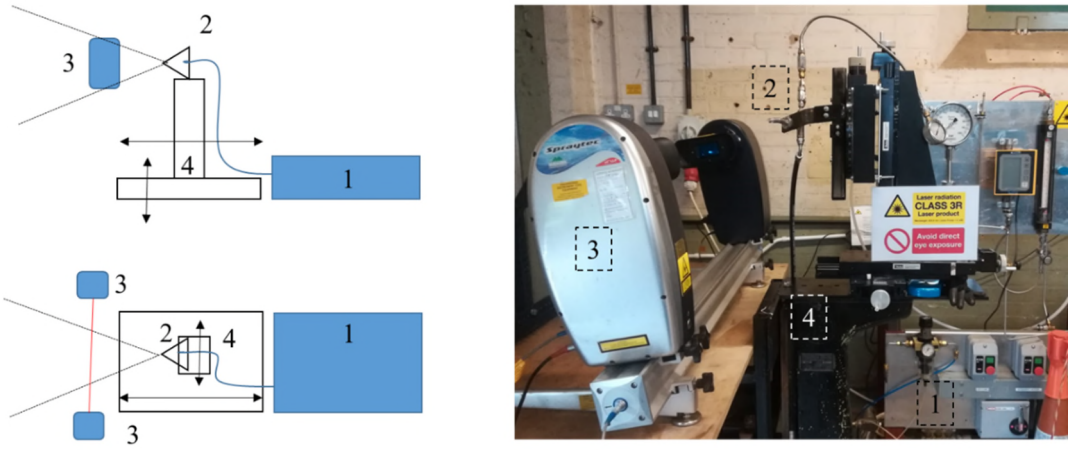

Figure 2 Experimental set-up for single nozzle testing

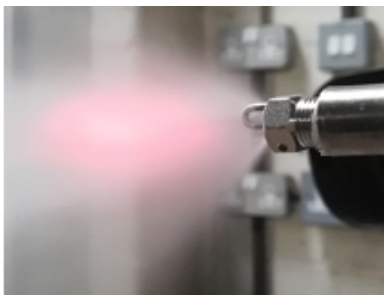

Figure 3 Impaction pin nozzle

2.2- Uncertainty

Controlling the nozzle orientation proved challenging because the thread on the nozzle and that on the pressure fitting did not always align to give the same nozzle orientation, and the pressure fitting could not be rotated. Impaction pin nozzles do not produce a symmetrical spray, however, Chaker [34] evaluates the effect of this asymmetry at different pressures and flow rates and concludes that at high pressures, the droplet distribution is independent of the nozzle orientation. The current test set-up, did not allow for this to be confirmed, as there was no way of rotating the nozzle. For multi-point measurements, the nozzle was moved up and down with respect to the laser, so that the plume measurements could be taken at the "top", "bottom" and "centre" of the spray. When the nozzles were replaced, these measuring positions were repeated and controlled to an accuracy of ±0.1 mm. Despite this, the fog produced by the spraying nozzle slightly varied in shape. Some nozzles produced a plume with a slightly wider spray angle. Hence, the relative position between the laser and the "top" or "bottom" of the spray was not always the same. The thermocouples and pressure transducers used have an accuracy of 0.75% and 0.5% respectively, and that of the water flow meter is 2%. The temperature of the water and the air was constantly monitored to ensure that the difference between them stays within an acceptable range (<10°C). The temperature and humidity effects were studied by Chaker et al. [26] and concludes that the ambient conditions have minimal effect on droplet size decay and that this is rather dominated by the coalescence and break-up of the water droplets. The ambient temperatures at which the tests were conducted in the present study were in the range of 16- 19 °C.

2.3- Considerations for Single Nozzle Testing

The tests in the first part were conducted for single nozzles spraying water into the still air. Since the intention is to subsequently use the nozzles in a manifold for the engine test, 8 identical nozzles were tested individually to quantify the similarity between them to characterize the spraying fog. The initial measurement position was taken at centreline and traversed in 50 mm intervals, going from 50 mm away from the nozzle up to 700 mm. No significant change in droplet diameter was observed beyond 150 mm from the nozzle. This is in agreement with Chaker et al.[26,30]. In both studies, the droplet size was reported to stabilize after 100 mm. The standard for inlet fogging [32] recommends the readings to be taken at 75 mm away from the nozzle. However, the droplet size distribution was seen to increase beyond 75 mm; stabilization of the measurements was only observed at 100 mm and beyond. For this reason, the initial measurements were taken as close as possible from the nozzle (50 mm) similar to Ref.[35]. The measuring distance was then increased to 150 mm and 250 mm. The vertical distribution of the plume was also varied, considering 2 other radial positions other than the centre position: + 20 and - 20 mm at the point closest to the nozzle. This distance was increased as the measuring position moved away from the nozzle tip, to follow the conical shape of the fogging plume. This is applicable for all the axial positions and controlled for an accuracy of 0.1 mm. Since commonly used injection pressures in industrial systems are between 69 and 138 bar, only this range is considered here.

Water injection causes an increase in the humidity of the surrounding air that subsequently has a higher index of refraction than dry air. This causes extra light diffraction, which leads to the receiver reading high light incidence angles. The consequence of this is a larger estimation of droplet sizes than they actually are. This phenomenon is known as beam steering [31] and the ASME standard for water spray measurement [32] recommends restricting the droplet diameter range to 200 μm, to reduce the influence of this effect. However, the laser manufacturer recommendation is to identify the detectors in the receiver

that are affected by beam steering and turn them off. The light scattering pattern will change as a result of this. However, the processing software is embedded with an algorithm that corrects for the missing detectors; the exact details of this correction are not provided by the manufacturer. Both approaches were tested to evaluate the influence on the results, as presented subsequently. For both approaches, a background reading of the media (air) and ambient light is taken prior to the start of the spraying and droplet measuring.

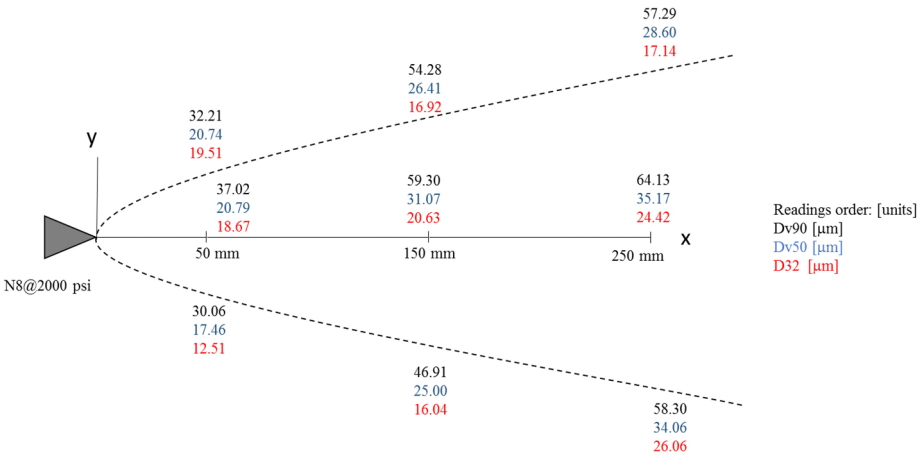

Figure 4 Droplet distribution across the plume at 138 bar

Figure 4 depicts the measurements taken at the 9 locations in the x (50, 150, 250 mm) and y coordinates, for one of the nozzles tested at 138 bar. The figure shows a general increase in the droplet diameter with an increase in axial distances away from the nozzle exit. Although the size diameters are similar between the axial locations, the figure shows the importance of measuring at different points across the plume. Some studies have identified smaller droplets at the "centre" of the plume, and larger droplets at the edges [35]. This is not the case observed in this study due to the presence of the spray cone edges as shown in Figure 4. The first set of readings from the left (Figure 4), taken at 50 mm away from the nozzle shows a Dv_{90} of 37.02µm at the centre, but 32.21µm and 30.06µm at the top and bottom of the spray (in black ink). When measuring the conical-shaped spray at any "y" position, the laser travels through the edges and centre of the plume, penetrating the cloud across the "z" direction as illustrated in Fig. 5. This means that the readings taken will account for the edges and the "core" of the conical spray. To mitigate this effect and account for a more indicative reading at the core or centre of the spray, a separate set of measurements was taken by "shading" the edges of the spray, using an obstruction as shown in Figure 5. For a given (x, y) position of (50, 0) mm, the droplet diameters (Dv_{90}) measured at the core of the plume were about 45% smaller than those seen when the measurements were conducted without the obstruction of the spray cone. This observation served to explain the findings of smaller droplets at the core of the plume, obtained in other studies. Nevertheless, in the present study, these "core" readings were not used for further analysis, as the measurement taken with full cone penetration provide a more indicative sizing of the droplet diameter in this region.

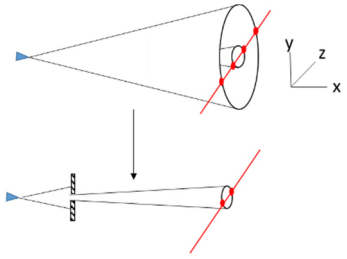

Figure 5 Spray without and with shading/obstruction of the edges

3- Results for Droplet Size Analysis

If the transversal values of Fig.4 (y_1,y_2,y_3) are weight averaged, the plume can be characterized by only three values for the 3 axial distances from the nozzle (50, 150 and 250 mm). Figure 6 shows the influence of varying measurement distance for the case of 5 nozzles. As expected, the droplet size increases with increasing distance from the spraying point. This behaviour was noted by Refs. [30,36] and it is attributed to droplet coalescence and the evaporation of smaller droplets. On average, a smaller increase in droplet size is seen to occur when moving from 150 mm to 250 mm.

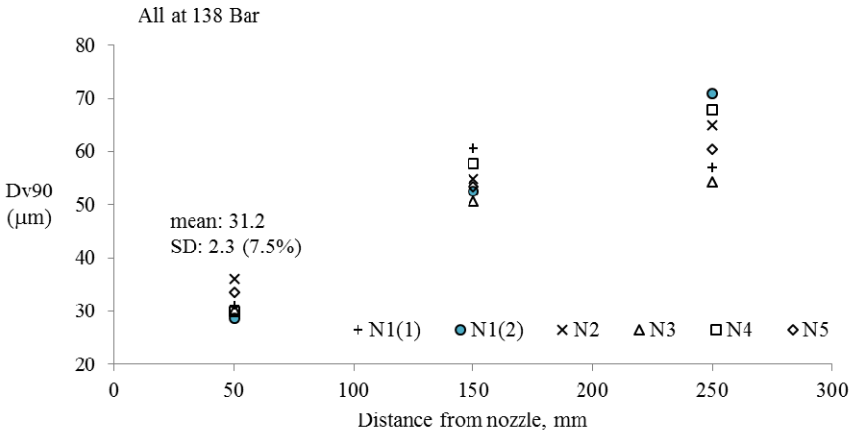

Figure 6 Influence of measuring distance on droplet size

The figure also shows the cases for which the droplet size diameter is restricted N1 (1) and when the detectors are turned off N1 (2). No significant difference was noticed between the methods, and so the latter was selected. The apparent decrease in diameter of N1 (1) when moving from 150 to 250 mm has to do with the coalescing and bouncing phenomenon. Since evaporation has stopped in this region due to the saturation of the air and extinction of small droplets, from 150 mm onwards the droplet size is governed by the droplets braking, merging or bouncing that is a stochastic process. In the case of N1, it is possible that the measurement taken at 250 mm was in a region where droplet merge was less dominant; hence the distribution shows a slight decrease in droplet size. Initially, all droplets exit the nozzle at the same speed, but as they travel away from the injection point their speed reduces due to a loss in momentum caused by a reduced mass that is accompanied with a continuous air drag resistance. Hence, initial smaller droplets slow down faster than larger droplets due to a lower initial momentum. The low-energy droplet impacts that occur in the region away from the nozzle are responsible for droplet coalesce rather than bounce. This phenomenon is responsible for the higher droplet sizes observed (with larger deviations) farther away from the injection point.

The measurement of all the particle sizes had a standard deviation of 2.3 μm at 50mm from the nozzle, and 5.1μm and 5.3μm at 150 and 250 mm respectively. Considering the mean diameters of 31, 56 and 63 μm, the standard deviation (SD) at any one point is below 10% of the mean. This was considered acceptable for the current set-up, in agreement with the ASME standard for fogging nozzles [32]. Results of the mean values of all the nozzles at the three distances are presented in Figure 7 for pressures of 69 and 138 bar, with the corresponding error bands. The SD presented in the figure as a percentage, (7.5, 9.2, and 8.5%) is applicable to the 138 bar case. It can be noted that doubling the pressure has a small effect on the droplet diameter reduction as observed by Refs [30,37]. According to Ref. [37], impaction pin nozzles have much less influence from injection pressure than pressure swirl nozzles. In the study, the authors report a 20% reduction in diameter for a three-fold increase in injection pressure. For a similar kind of nozzle at 138 bar and at 50 mm away from the nozzle, the study reports a mean diameter of 29.8 μm (2% smaller than the mean reported here, but still within the range of the SD). Chaker [30] reports a smaller Dv_{90} of around 28μm but with an airspeed of 1 m/s. The SD for the 69 bar case for the three points analysed here were 9.4, 9.5 and 6.5% respectively.

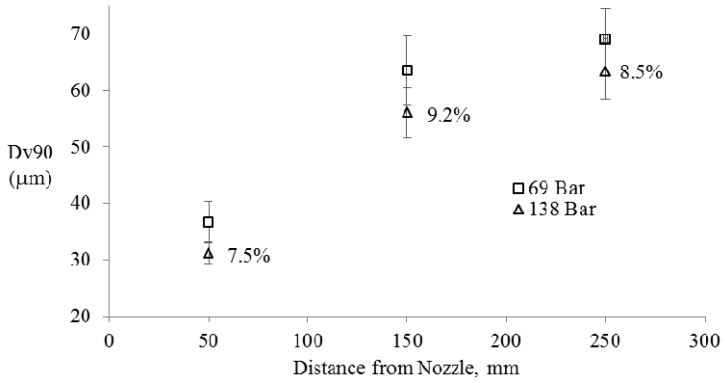

Figure 7 Droplet Diameter with distance for different injection pressure - mean values presented

The investigated effect of water temperature is shown in Figure 8. The figure indicates the minimal influence of water temperature on droplet diameter, as also observed by Ref. [27,36]. These Dv_{90} and D_{32} measurements were taken at 150 mm from the nozzle, over a period of 10 minutes by spraying water as it was gradually heated. The interest of this was to identify any favourable temperature that can bring about a further reduction in the droplet sizes.

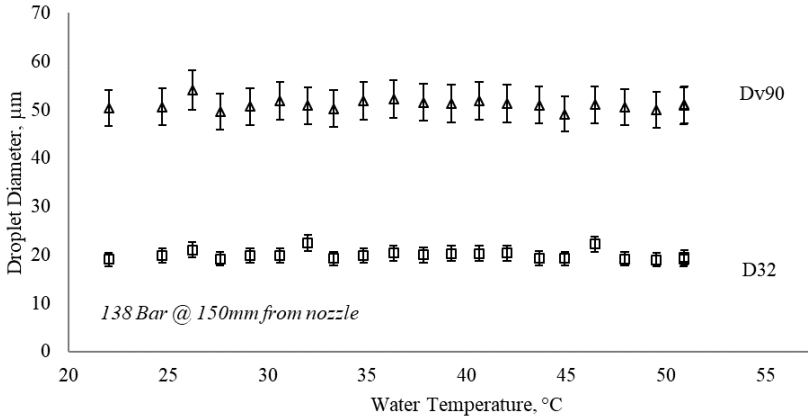

Figure 8 Influence of temperature on droplet size

This first part served as a basis for understanding the droplet size distribution and behaviour for a single nozzle before progressing to the case of a multi-nozzle arrangement that is necessary to achieve the required water-to-air ratio. Other efforts made to arrive at the selected injection pressure and nozzle type are indicated in Fig A1 of Appendix A. The figure shows the relationship between the nozzle type and injection pressure. The requirement for smaller droplet formation allows for better intercooling inside the compressor thereby reducing the temperature of the gas path of the engine. This relatively cooler operation reduces the endothermic NO_x emissions as explained by Block and Igie.[12]. Smaller droplets also reduce the risk of blade impingement which could lead to surface erosion and a loss in the aerodynamic efficiency.

4- Gas Turbine Engine Testing

4.1 Experimental Set-up

The water injection rig along with the laser and a multi-nozzle manifold was then installed in front of a single shaft gas turbine engine as shown in Figure 9. The figure depicts the engine intake (1), the laser (2) and the spraying nozzles (3). Water was injected into the engine at varying water-to-air ratios (f) but at a fixed injection pressure of 138 bar. The water quantity was controlled by the number of nozzles; 1 nozzle delivers water at 0.166% of the air mass flow, while 3, 6 and 12 nozzles amount to 0.5%, 1% and 2% respectively.

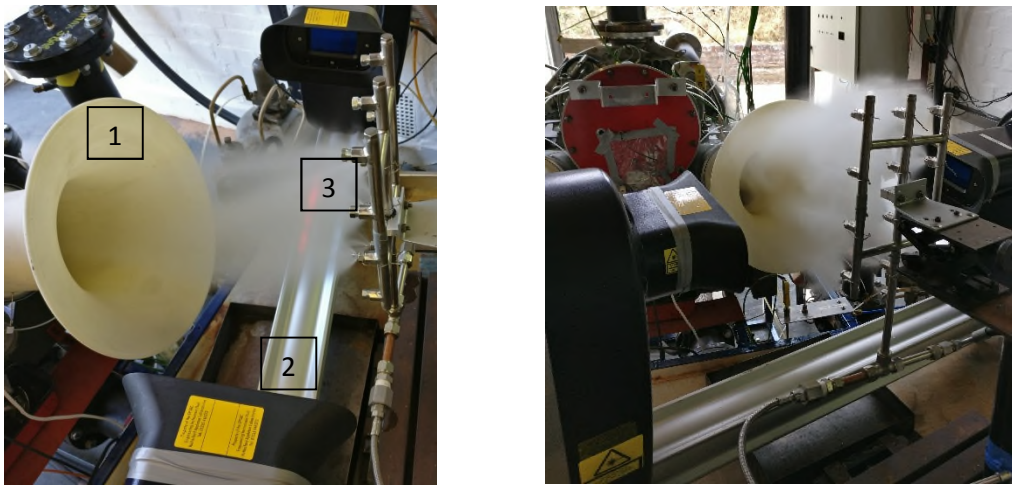

Figure 9 Photograph of the experimental set-up. Engine Intake (1), Laser (2), and Nozzles (3)

The Rolls Royce *Artouste* gas turbine engine was deployed to investigate the effects of compressor water injection. This type of auxiliary power unit (APU) was used to provide compressed air to start the main aircraft engines like the Rolls-Royce Conway – the first turbofan to enter into service- that powered some versions of the Vickers VC10 and Boeing 707-420 [38]. The *Artouste* engine as described in Figure 10 consists of a single-stage centrifugal compressor (on the right-hand side of the figure), an annular combustion chamber and a two-stage axial flow turbine that is directly coupled to the centrifugal compressor on the same shaft. Some measured and calculated performance parameters of the "dry" engine condition are presented in Table 1. This includes the total inlet air temperature (T_{in}) and pressure (P_{in}), Compressor Discharge Temperature (CDT), Exhaust Gas Temperature (EGT), air mass flow, (m_{air}), Fuel Flow (FF) and Pressure Ratio (PR) for which the measurement stations are depicted on Figure 10. The table shows on the left-hand side column the averaged performance parameters corresponding to the "dry" tests, and on the right-hand side, the corresponding averaged and corrected values. The latter is the result of averaging over 7,000 readings over a period of time and then correcting them to ISA temperature and pressure (Eq.2) [20,39].

$$\theta = \frac{T}{288.15} \qquad \delta = \frac{P}{101.325} \tag{1}$$

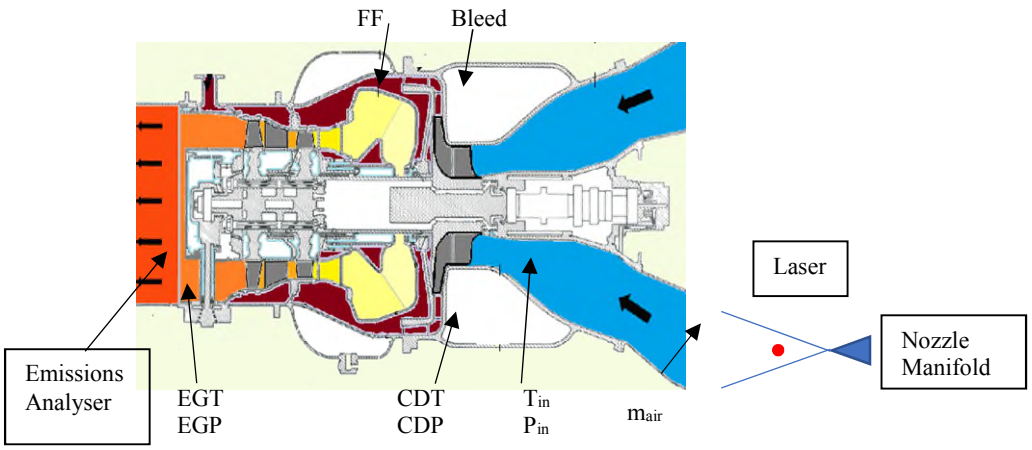

Figure 10 Gas Turbine Experimental Set-Up. Adapted from [40]

The temperature and pressure based corrections do not account for the relative humidity (60% used for sea level stationary gas turbines). Igie et al.[41] devise an extended correction accounting for relative humidity effects. This shows that the influence is very small for the range of temperatures investigated in this study and hence can be neglected for the data correction. In this investigation, the engine is operating without any load or driven equipment and hence there is no power requirement or demand. It is also important to mention that the performance of this engine is unlikely to exactly match the manufacturer's design specification even at the same ambient conditions and rotational speed. This is mainly due to mechanical wear and tear and refurbishments over the years of service. As such, the reference conditions applied here for water injection are corrected conditions before and after water injection is applied.

Table 1 Performance at dry engine condition (averaged, and corrected values to ISA 288K and 101325Pa)

	Averaged Measurements	Averaged Measurements corrected to ISA
Tin (K)	303.3	288.0
P in (kPa)	100.6	101.3
CDT(K)	471.9	449.0
EGT(K)	795.3	756.0
FF (kg/s)	0.034	0.0332
n (RPM)	33096.0	32261.0
Ma (kg/s)	3.2	3.3
PR	3.4	3.4
Cw (kW)	172.6	164.2
Measured Dry Emissions	NOx: 40.28 ppm CO:446.57 ppm CO_2: 3.23%	
Fuel Type:	Kerosene	

This experimental gas turbine is equipped with five k-type thermocouples; two at the intake, two at the compressor discharge and one at the turbine exit. The temperature measured by the thermocouples is the mixture temperature, as there was no way to condense the extra water. Pressure transducers were used to evaluate the static and total pressures at the same stations (the compressor inlet and bleed duct) using a pitot-static tube. At the exit of the compressor, pressure tapings are installed to a manometer that measures

the gauge pressure. As such, the absolute pressure is calculated to obtain CDP. These readings were used to calculate the parameters on the bottom columns of Tab. 1. The accuracy and errors of the instruments are the same as for section 2.2. At the exit of the turbine, a Protea ProtIR 204M ® emission analyser was installed as highlighted in Figure 10. This analyser is based on the Fourier Transform Infrared (FTIR) technology for stack emission testing. It has a resolution for NO, NO_2, CO and CO_2 of 0.9, 0.3, 0.2 and <2 ppm respectively. As a reference comparison, ICAO [42] recommends resolutions better than 1 ppm for NO_x, 2 ppm for CO and 100 ppm for CO_2, when measuring aircraft engine emissions. The emissions were collected by means of a probe installed at the exit of the engine. A suction pump collects a sample of the gas and mixes it in a dilution chamber prior to analysing the composition of the mixture. The analyser takes six readings before giving an output and this whole process lasts for around 60 seconds. The user can track this process and read each point measurement as well as track the history of each gas species. During the tests, the engine was left with unchanged conditions for a period of time long enough for the readings to stabilize, as the species of each gas changed when water was injected.

4.2 Water Droplet Measurements at the Engine Intake

The spraying nozzles were located 290 mm away from the compressor intake and the droplet diameter readings were taken at a distance of 50 mm away from the nozzle. Due to the presence of the engine bellmouth, the entrance of the compressor was inaccessible to the laser. As such, the water droplet diameters were measured at the exit of the nozzle and the change in size from the measuring point to the compressor inlet was estimated. Two approaches were selected to approximate the change in size from the nozzle exit to the compressor inlet: an empirical [30] and an analytical method [8]. The work presented by Ref [30] shows empirical correlations to predict droplet size change as a function of pressure, measuring position, airflow or water mass flow. The correlation presented in Eq. 2 is derived from experiments and depends on empirical parameters and a nozzle constant, k. The empirical constants were set to μ=0.23, δ=0.14, π=0.16, ω=0.14, as recommended by Chaker [30]. A similar correlation for the D_{32} can be found in the referenced study. In the stand-alone nozzle test (section 3), and for the position of 50 mm at 138 bar and at a given mass flow, a droplet size was calculated using Equ.2. This value was compared against the experimental readings taken at the same position. The difference between these two values determines the nozzle constant, k. An average was then made between all the measurements and k was chosen to be 491 for this type of nozzle. The correlations lead to errors mostly between 1.8 and 10% (and in a few cases up to 20%) when comparing the predictions with the actual measurements. The same maximum uncertainty of 20% was applied to predict the droplet sizes at the compressor entrance.

$$Dv_{90} = k\frac{m_w^{\mu} D^{\delta}}{\Delta P_w^{\pi} V_a^{\omega}} \tag{2}$$

When analysing droplet decay at still air and different air flow velocities, refs. [29,30,36] noticed that the size stabilizes after 10-12 m/s and also after 100 mm of leaving the nozzle. This is due to the air being saturated (no further evaporation) as well as the fact that the effect of coalescence and break up is diminished after the primary breakup phase. When applying Eq. 2 to moving air at 12 m/s and 50 mm away from the nozzle, a D_{v90} of 30± 6 μm is obtained. This compares well with the measured readings while the engine was running, which gave a D_{v90} of 35±2 μm. The distribution obtained at the measuring station also showed that 50% of the volume had droplets of 22±1μm or smaller (Dv_{50}=22) and 10% of the volume was distributed in droplets of 13±1 μm or smaller (D_{v10}). The stated distribution implies that 40% of the volume is represented by large droplets of size between 22 and 35 μm, which are not expected to fully evaporate in the compressor.

The values obtained at the measuring point were set as boundary conditions and applied to Equ.2 to predict the droplet size at the compressor inlet, 240 mm away from the measuring station. It was predicted that the droplets would have a Dv_{90} of 36 ±7 μm and a D_{32}=16 ±3μm. The droplet size was also estimated by means of a physics-based evaporative method [8,43]. These methods assume that the droplets evaporate until the air is saturated. Once saturation occurs (100% relative humidity) no further evaporation is possible. The analytical model does not consider coalescence or breakup and predicted a droplet size of 27 μm based on mass transfer-driven evaporation only. It can be noted that since the analytical model does not account for droplet coalescence, a lower droplet diameter is predicted. Details on the diameter reduction of an isolated droplet based on mass diffusion theory can be found in Ref. [43].

When using the maximum number of nozzles (12) corresponding to a water-to-air ratio of 2%, the fogging plume was too thick for the laser to achieve full penetration. Measurements were only possible for the configurations with 1, 3 and 6 nozzles, corresponding to water-to-air ratios of 0.13, 0.5 and 1%. There was a small increase in droplet diameter when using multiple nozzles attributed to the increased number of collisions between the droplets, leading to higher droplet coalescence. This increase is already accounted for in the size distribution discussed.

4.3 Engine Performance with water injection

The engine measurement data have been obtained simultaneously (including droplet size and exhaust emissions) and continuously as shown in Figure 11 for each set of experiments. After the engine was operated under dry conditions, different amounts of demineralised water were introduced ranging from 2% to 0.5% of water-to-air ratio. The engine was initially allowed to warm up for about 7 minutes before introducing water; this is well within the start-up time recommended by the manufacturer that suggests 40 seconds. Since the engine pressures and temperatures were recorded in real-time, it was straightforward to identify the stabilization of the readings before the water injection.

In reference to Figure 11, after minute 7, a quantity of water equivalent to 2% of the inlet-air-mass flow was injected into the compressor. The figure shows the changes in the four parameters mentioned in Tab. 1, when the engine is injected with 2%, 1% and 0.5% of water. Figure 11 also shows the raw data (fluctuating lines) and the time averages for each quantity. At each engine operating condition, around 700 individual readings for pressure and temperature were taken. The mean of these values (presented as a continuous line superimposed on the raw data) and standard deviation (SD) were computed. The SD seen for each set of readings was noticed to be below 1% of the mean. Further statistical analysis of the raw data is presented in Appendix B.

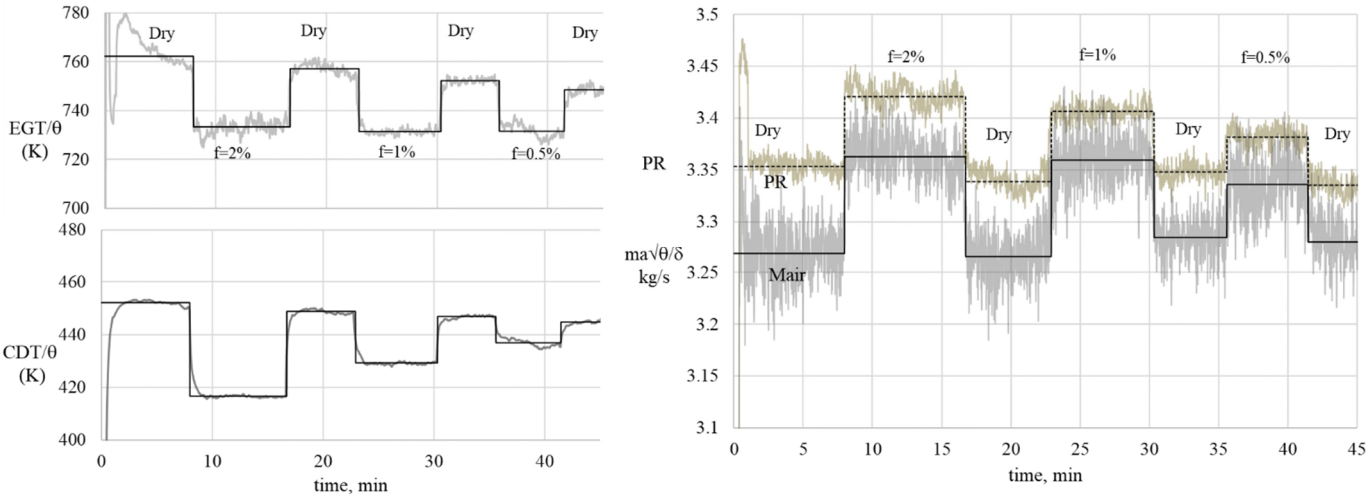

Figure 11 Raw and time-averages of CDT, EGT, PR and mass flow

Figure 11 shows a significant decrease in CDT and EGT immediately after the injection was initiated. For 2% injection, this amounts to average values of 36 K and 29 K respectively. These reductions in temperatures increase the air density which in turn increases the air mass flow rate (continuous line) and pressure ratio (dashed line) indicated in Figure 11- Right. For the interpretation of the results, it is important to indicate that the engine is operating at an approximately constant rotational speed; as a result, the shaft torque will increase with air and fuel flow increases. Subsequent injection of water at reduced injection rates shows similar benefits but at a lower magnitude of change. It is important to note that a reduction of injection rate by half does amount to almost half the benefit of performance improvement. For example, the drop in corrected CDT of 2%, 1% and 0.5% are: 36 K, 19 K and 10 K. That of the rise in corrected mass flows is 3.1%, 2.8% and 1.5% respectively, with the reference dry condition being that prior to the injection of water for each case.

Only the key investigation of 2% injection rate was conducted with the most number of runs – 7 experimental cases - as indicated in Table 2. The values are computed from averaging each reading during the time that water was injected, and comparing this with its corresponding "dry" value. The table shows the changes in performance parameters, inclusive of the specific compressor work for all the experimental runs. The corrected compressor work reduces as shown in Tab. 2 and the calculation is explained subsequently. Also presented are the mean values of the readings and their standard deviation. Considering that the thermocouples and pressure transducers can give measurement errors of 0.75% and 0.5% respectively, the variation seen between each experiment is acceptable.

Table 2 Changes in Engine Parameters with 2% water injection ratio

	CDT/θ (K)	EGT/θ (K)	maθ/δ (%)	PR (%)	Wc/θ (%)
Exp 1	-32.0	-33.7	3.9%	2.9%	-10.0%
Exp 2	-32.0	-37.7	3.0%	2.2%	-8.5%
Exp 3	-38.3	-33.1	2.8%	2.5%	-10.3%
Exp 4	-33.0	-37.2	3.0%	1.9%	-8.1%
Exp 5	-34.6	-23.9	3.0%	2.4%	-9.4%
Exp 6	-35.5	-28.8	2.9%	2.0%	-9.7%
Exp 7	-32.6	-26.8	2.8%	2.2%	-11.4%
Mean	-34.0	-31.6	3.0%	2.3%	-9.6%
SD +/-	2.2	4.9	0.3%	0.3%	1.0%

The specific calculated compressor work (W_c) presented on Tab.2 and subsequent figures are the comparison between the "wet" and "dry" specific compression work. These two are calculated in a different way and arise from different assumptions. When water is injected, the pressure ratio will increase, along with the mass flow. The wet compression work thus has to be compared to the dry compression work but at the new pressure ratio (and mass flow for compressor power). To do this, the compressor inlet, outlet temperatures and pressure ratio are used to calculate the polytropic efficiency of the compressor. Then, assuming the efficiency stays constant, the dry work is re-calculated at the "wet" pressure ratio but assuming "dry" compression. This value is then corrected to account for inlet temperature variations by using the dimensionless factor, θ (Eq.1).

The wet compression work is calculated by adding the enthalpy changes of water vapour, dry air and liquid water as seen on Eq. 3.

$$(\dot{m}_a h_a + \dot{m}_v h_v)_1 + \dot{m}_{w1} h_{f1} + w_c = (\dot{m}_a h_a + \dot{m}_v h_v)_2 + \dot{m}_{w2} h_{f2} \quad (3)$$

The wet compression work (W_c) is then defined by,

$$w_c = C_{pa}(T_2 - T_1) + w_2(C_{pv}T_2 + h_{fg}) - w_1(C_{pv}T_1 + h_{fg}) + f_2 C_{pf} T_2 - f_1 C_{pf} T_1 \quad (4)$$

Where subscript 1 and 2 denote the entry and exit of the compressor respectively. T is the measured total gas temperature, w, the entry and exit water vapour content (specific humidity) of air, f, the liquid water-to-air ratio. $C_{Pa,v,f}$ are the specific heat capacities of air, water vapour and liquid water, taken constant and equal to 1005, 1820, and 4180 kJ/kg. The entry conditions of liquid water and water vapour are known and can be measured at the intake; however, the exit humidity of the air and the amount of unevaporated water cannot be measured. This is estimated by measuring the compressor exit temperature and calculating the amount of water that would need to evaporate to cause that decrease in temperature. Taking the thermodynamic model presented in Refs [8,44], the following equation can be derived to calculate the amount of evaporated water; which, by mass conservation, will be equal to the increase in specific humidity of the air.

$$dw = \left(\frac{\ln(PR)}{\ln(TR)} - \frac{\gamma}{\gamma - 1} + \frac{(n_{poly} - \gamma)}{(\gamma - 1)(n_{poly} - 1)}\right) * \frac{R_a}{h_{fg}}(T_2 - T_1) \quad (5)$$

Where PR is the pressure ratio (P_2/P_1), TR the temperature ratio (T_2/T_1), γ, the specific heat ratio, R_a, the gas constant of air, h_{fg} the heat of vaporization of water, and n_{poly} is a constant related to the polytropic compressor efficiency η_{poly} [32],

$$n_{poly} = \frac{\eta_{poly}\gamma}{\eta_{poly}\gamma - \gamma - 1} \quad (6)$$

Equations 5 and 6 are derived from an energy balance across the compressor and removing the adiabatic condition. Instead of assuming an adiabatic process, it is assumed that there is a heat transfer term, which equates to the latent heat of evaporation that is absorbed by the water. The reader is referred to ref. [8,44,45] for further details on the derivations of these equations. An estimation of the unevaporated water is then obtained using Eq. 5. The water vapour and liquid water fractions are then used in Eq.4 to calculate the wet compression work.

Figure 12 shows the same engine parameters as Tab.2 but this time for different water-to-air ratios (0.5 - 2%). The figure also includes the error bands for the cases with the highest amount of experiments (1, 2%), derived from the standard deviation of the samples. The case for 0.5% does not include graphical

error bands as the sample size was smaller (3 experiments). As stated above, 7 experiments were done for the largest amount of ingested water (2 %) and 5 experiments were conducted for the case with 1 %. The mean percentage change of each parameter is displayed for extra clarity. All the values presented have been corrected to ISA conditions and were taken at a frequency of 1 Hz. The presented values are representative of over 7,000 data points taken at each operating condition (See Appendix B for more information). The bleed air from the compressor was always kept the same.

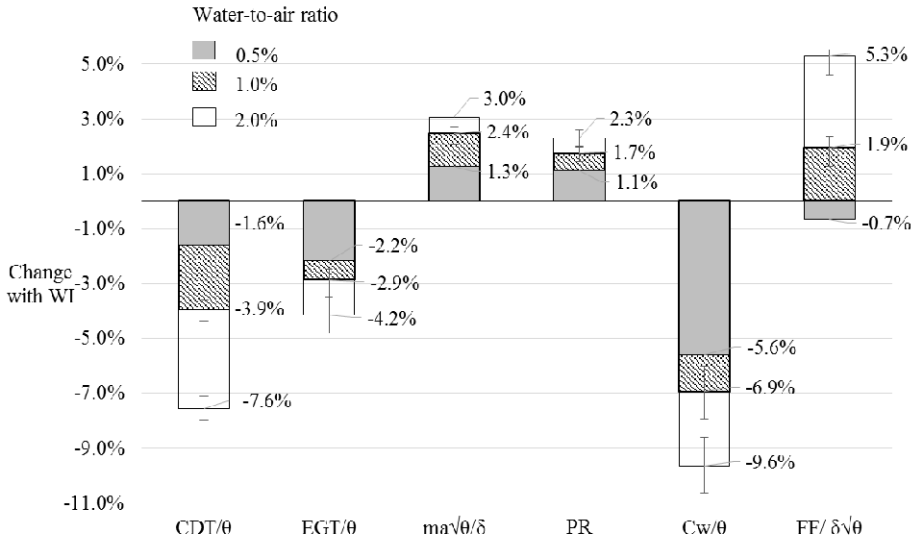

Figure 12 Engine parameter changes with water injection at different water-to-air-ratios (0.5-2%)

As expected, higher water injection ratios cause higher temperature reductions resulting from the increased amount of water in use, hence the corresponding corrected mass flow rise shown in Figure 12. The corrected fuel flow also increases with the amount of injected water, though at a higher magnitude. As such, this increase in the fuel-to-air ratio could bring about a rise in the combustor exit temperature that is not directly measured. However, this is not the case since the evaporation of water is still expected to take place in this combustor due to the relatively low operating temperature and pressure of the compressor. This increase in fuel-to-air ratio observed is consistent with other findings of combustor water injection previously discussed. However, this is not the case for 0.5% injection ratio where the least amount of water is used, suggesting a predominant effect of compressor intercooling (less water reaches the combustion chamber). This is evident by the fact that the compressor specific work reduction is high for the low water-to-air ratios compared to what is achieved when the amount of water is doubled from 0.5% to 1%. The amount of water exiting the compressor can also be estimated using Equ. 5 and the measured CDT. It is important to reiterate that the performance benefits of compressor intercooling are also prevalent at the high injection rates and signified by the drop in CDT and specific work of the compressor in these cases. The compressor work shows large uncertainties compared to the CDT, mass flow and PR. This arises from the fact that the compressor work is dependent on two measurable properties: the temperature and pressure. In addition, the calculation of evaporated water (from Eq.5), needed for estimating the wet compression work adds to the uncertainty.

For the cases of increased corrected fuel flow, more torque is expected to be produced at the turbine. Higher actual turbine work, in turn, increases the compressor power that is indicated by the rise in pressure ratio. Nevertheless, the compressor does less specific work (in comparison to the increased mass flow) due to the increase in density resulting from intercooling. The standard deviation seen for the EGT was

larger than that seen for the CDT, mainly because the EGT was measured at only one position, while the former was measured in two locations and averaged. It is expected that the temperature distribution at the exit of the engine will not be uniform and so an improvement to these conditions would be to measure at circumferential and radial positions across the exit of the engine as recommended in Ref. [20].

The behaviour of the engine is linked to the way in which it is operated. Previous studies [12], considered the modelling of a turbofan engine under compressor water injection. In the analysis, the constraint was the thrust which was kept constant when injecting water. For this operation, the engine rotational speed and compressor specific work would reduce. The thermodynamic efficiency of the engine improves as a result of the reduced required fuel flow for the same useful work output (net thrust). An increase in the fuel-to-air ratio is applicable to both combustor and compressor water injection but with augmented power output or thrust. Studies on the latter show an increase of up to 20% in the useful work [46–48].

4.4 Emissions with water injection

The changes in NO_x and CO emissions as a percentage of the dry (ppmv) value are presented in Figure 13. The figure indicates that as more water is injected, the NO_x emissions reduce further; and this is attributed to more cooling of the engine. The highest reduction of 25% occurred at 2% water-to-air ratio is a case for which more water entered the combustor, as such, the CO emissions increased by about 41%. From the indicated droplet distribution previously discussed, more than 40% of the injected water volume was measured to have droplets between 22 and 35μm. These droplets are not expected to fully evaporate in the compressor and thus will reach the combustor. The unevaporated water attempts to quench the flame and brings about a reduction in combustion efficiency; a phenomenon experienced when injecting water directly in the combustor [49,50]. The magnitude of these changes decreases with reduced water-to-air ratios. In this study, the TIT is not measured but expected to drop slightly (based on the inference from the decreases in NO_x) and the power output is increased, as signified by the increase in PR and fuel-to-air ratio cases.

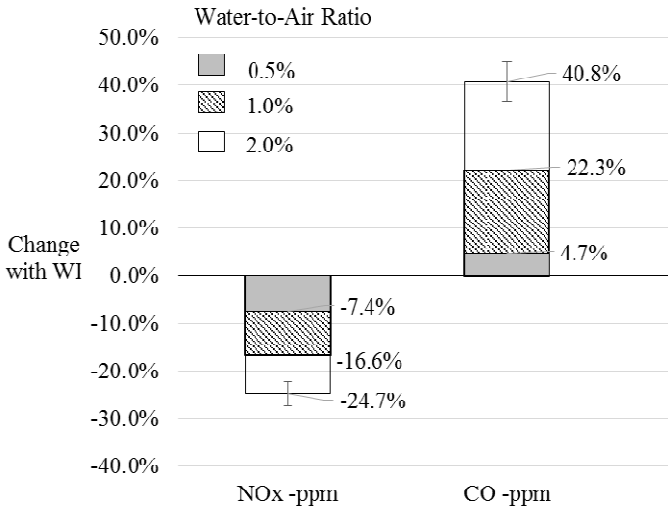

Figure 13 NOx and CO changes with water injection at 0.5, 1 and 2%

Other studies as discussed in the Introduction have obtained greater reductions in NO_x emissions. This is mainly a result of the operating temperature and pressures of these larger engines. With respect to compressor water injection, the larger engine compressors are more favourable, operating with a CDT that

is about twice the value recorded here and with at least 10 times the PR. It is rarely the case that there would be significant unevaporated water reaching the combustors with these same droplet sizes or injection conditions. For the combustor, large civil aircraft reach peak combustor temperatures of about 1,800 K, leading to greater NO_x production. However, these operating temperatures present more beneficial conditions for water injection. A 2-spool turbofan with a take-off PR of 30.5 has a NO_x Emission Index of 33 gNO_x/kg of fuel. During idle, at low power settings, this value drops to 4.5 g/kg due to the low operating temperatures and pressures [51]. The engine considered here has a "dry" emission index of 2.9 g/ kg; as such it already produces considerably less NO_x at baseline than what would be noted on a large engine.

5- Conclusions

This work has examined an impaction pin nozzle spray characteristics at different injection pressure and water temperature, alongside the impacts of injecting generated droplets into the compressor, as well as further ingestion into the combustor to reduce NO_x. The first part of the study shows smaller droplets generated when the higher injection pressure is used. This effect is seen to change axially and transversely, away from the nozzle. The influence of water temperature ranging from 288 K to 325 K is seen to have no influence on the droplet size generated.

For the engine tests, the highest water pressure was selected (138 bar) and the nozzles were installed at the engine's intake. The droplet size at the exit of the injection nozzle was measured and the droplet size at the engine intake was estimated at 37μm (Dv_{90}) based on correlations. This study shows that injecting 2% of water by mass flow had the following effects on engine performance:

- Reduces the CDT by up to 34K (7%) and EGT by up to 29K (4%).
- Increases pressure ratio and mass flow by up to 2.3 and 3% respectively.
- Increases the fuel-to-air ratio by 2.2% that is associated with the 40% rise in CO.
- NO_x reduces by 25%.

The amount of NO_x reduction at high water-to-air ratios are attributed to a dominant combustor effect, while that of the least amount of water used is mainly based on the compressor effects. In all cases, the compressor specific work and CDT reduces, and the pressure ratio rises, owing to the benefit of compressor water injection on the performance. As shown in analytical studies of compressor water injection, reducing the droplet sizes further will bring about an improvement in the stated parameters.

The present work can serve as a validation case for future numerical simulations on this engine type while serving as evidence of emissions reduction potentials for larger engines. Experimental studies are required, especially in the area of the modern turbofan engines with axial flow compressors, where water injection appears to be more favourable. The small size of the engine investigated causes continuous evaporation from the compressor through to the combustor, that is not likely to occur for larger engines at these water-to-air ratios. The utmost reductions of NO_x for compressor only cooling are expected to be when the same required thrust or power is achieved (rather than augmentation), that will bring about a reduction of the fuel utilised.

Acknowledgements

This work was supported by the Mexican National Council for Science and Technology (Conacyt). The authors owe gratitude to Thomas Mee III, Scott Booden, Dr.Ioannis Roumeliotis, Paul Lambart and Natan Zawadzki for their technical support.

Nomenclature

APU	Auxiliary Power Unit	η_{poly}	Polytropic efficiency
ASME	American Society of Mechanical Engineers	ICAO	International Civil Aviation Organization
CC	Combustion Chamber	ISA	International Standard Atmosphere
CDT	Compressor Discharge Temperature	K	Nozzle characteristic constant
CO	Carbon Monoxide	μ	correction factor- mass flow
CO_2	Carbon Dioxide	m_a	Air Mass Flow
C_p	Specific heat (J/ kg K)	m_w	water mass flow
D	Distance from the nozzle	NO_x	Nitrogen Oxides
δ	correction factor- distance	n_{poly}	polytropic coefficient
δ	Pressure Correction factor P/Pisa	π	correction factor- pressure
D32/ SMD	Sauter Mean Diameter	P	Pressure
Dv 10	Droplet diameter: 10% of the volume	ppm	Parts Per Million (Volume)
Dv 50	Droplet diameter: 50% of the volume	PR	Pressure Ratio
Dv 90	Droplet diameter: 90% of the volume	Pw	Water Pressure
EGT	Exit Gas Temperature	θ	Temperature correction factor T/Tisa
EI	Emission Index	Ra	Specific gas constant of air 287 J/kg K
f	injection ratio, %	RPM	Revolutions Per Minute
FF	Fuel Flow	SD	Standard Deviation
FS	Flat Spray	T	Temperature
FTIR	Fourier Transform Infrared	TIT	Turbine Inlet Temperature
γ	Air specific heat ratio, 1.4	TR	Temperature Ratio
h	Specific enthalpy (J/kg)	Va	Air Velocity
HC	Hydro Carbons	WAR	Water-To-Air Ratio
h_{fg}	Heat of vaporization of water 2500 kJ/kg	ω	correction factor- air velocity
HC	Hollow Cone	w	specific humidity
IP	Injection Pin	w_c	Compressor Specific Work

References

1. Future AS. ICAO Environmental Report 2016. 2016;

2. EEA (European Environment Agency). European Aviation Environmental Report 2016. 2016. Available at: DOI:10.2822/385503

3. Block N. DA., Igie U. Case For Exploring Compressor Water Injection For Airport Emission Reduction GT2017-64780. In: ASME (ed.) Asme turbo expo: Power for land, sea and air. Charlotte: American Society of Mechanical Engineers (ASME); 2017. p. TBC.

4. Mishra A. Aviation Environment Circular 1 of 2013. General of Civil Aviation. New Delhi; 2010.

5. Deonandan I., Balakrishnan H. Evaluation of Strategies for Reducing Taxi-out Emissions at Airports. 9th AIAA Aviation Technology, Intergation and Operations (ATIO) conference. 2010. pp. 1–14. Available at: DOI:10.2514/6.2010-9370

6. Liu Y., Sun X., Sethi V., Nalianda D., Li Y., Wang L. Review of modern low emissions combustion technologies for aero gas turbine engines Committee on Aircraft Engine Emissions Committee on Aviation Environmental Protection Committee on Aircraft Noise. Progress in

Aerospace Sciences. Elsevier Ltd; 2017; 94(August): 12–45. Available at: DOI:10.1016/j.paerosci.2017.08.001

7. Grönstedt T., Rolt A., Tantot N., Xisto C., Donnerhack S., Schmitz O., et al. Ultra Low Emission Technology Innovations for Mid-Century Aircraft Turbine Engines. ASME Turbo Expo: Turbomachinery Technical Conference and Exposition. 2016. pp. 1–13.

8. Block Novelo DA., Igie U. Aero engine compressor cooling by water injection - Part 1: Evaporative Compressor Model. Energy. 2018; 160: 1224–1235. Available at: DOI:10.1016/j.energy.2018.05.171

9. Sun L., Zheng Q., Li Y., Luo M., Wang J., Bhargava RK. Numerical Through Flow Simulation of a Gas Turbine Engine With Wet Compression. Asme turbo expo: Power for land, sea and air. Copenhagen; 2012. pp. 1–13.

10. Sun L., Sun T., Wang Y., Yang W. Numerical Simulation of Pollutant Emission of A Turbojet Engine with Water Injection. ASME Turbo Expo 2016: Turbomachinery Technical Conference and Exposition GT2016. Seoul; 2016. pp. 1–9.

11. Daggett DL., Ortanderl S., Eames D., Berton JJ., Snyder CA. Revisiting Water Injection for Commercial Aircraft. World Aviation and Exposition. Reno, USA; 2004.

12. Block Novelo DA., Igie U. Aero engine compressor cooling by water injection - Part 2: Performance and emission reductions. Energy. 2018; 160(x): 1236–1243. Available at: DOI:10.1016/j.energy.2018.05.171

13. Utamura M., Takehara I., Horii N., Kuwahara T. A New Gas Turbine Cycle for Economical Power Boosting. The American Society of Mechanical Engineers. 1997; 97-AA-142: 1–10.

14. Utamura M., Takehara I., Karasawa H. MAT, a novel, open cycle gas turbine for power augmentation. Energy Conversion and Management. 1998; 39(16): 1631–1642. Available at: DOI:10.1016/S0196-8904(98)00088-0

15. Jolly S. Wet compression - a powerful means of enhancing combustion turbine capacity. Power-Gen International. Orlando, Florida; 2002.

16. Roumeliotis I., Mathioudakis K. Water Injection on Compressor Stage Operation. Transactions of ASME. 2007; 129(July): 778–784. Available at: DOI:10.1115/1.2718223

17. Schnitzler JP., von Deschwanden I., Clauss S., Berna F., Dohmen HJ., Werner K. Experimental Determination of a Four Stage Axial Compressor Map Operating in Wet compression. ASME Turbo Expo 2014: Turbine Technical Conference and Exposition. Dusseldorf; 2014. pp. 1–10.

18. Munari E., D'Elia G., Morini M., Pinelli M., Spina PR. Stall and Surge in Wet Compression : Test Rig Development and Experimental Results. Journal of Engineering for Gas Turbines and Power. 2019; 141(July): 1–12. Available at: DOI:10.1115/1.4042474

19. Bahr DW., Lyon TF. NOx Abatement In Aircraft-Derivative Turbine Engines. The American Society of Mechanical Engineers. 1984; 84-GT-103.

20. Walsh PP., Fletcher P. Gas Turbine Performance. 2nd edn. Oxford: Blackwell Science; 2004. 646 p.

21. Shahpouri S., Houshfar E. Nitrogen oxides reduction and performance enhancement of combustor with direct water injection and humidification of inlet air. Clean Technologies and Environmental Policy. Springer Berlin Heidelberg; 2019; (0123456789). Available at: DOI:10.1007/s10098-019-01666-4

22. Daggett DL., Fucke L., Hendricks RC., Eames DJH. Water Injection on Commercial Aircraft to Reduce Airport Nitrogen Oxides. Nasa/Tm—2010-213179. 2010; (March).

23. C. W. Control of NOx Emissions from Industrial Gas Turbine Combustion Systems. A&WMA

Annual Meeting Vol.5. Anaheim, California; 1989.

24. William SB., Henderson RE. Aircraft Exhaust Pollution and its effect on the U.S. Air Force AD-783 828. Ohio, Wright Patterson Air Force Base; 1974.

25. Bhargava RK., Meher-Homji CB., Chaker MA., Bianchi M., Melino F., Peretto A., et al. Gas Turbine Fogging Technology: A State-of-the-Art Review—Part II: Overspray Fogging—Analytical and Experimental Aspects. Journal of Engineering for Gas Turbines and Power. 2007; 129(2): 454. Available at: DOI:10.1115/1.2364004

26. Chaker M., Meher-Homji CB. Gas Turbine Power Augmentation: Parametric Study Relating to Fog Droplet Size and Its Influence on Evaporative Efficiency. Journal of Engineering for Gas Turbines and Power. 2011; 133(9): 092001. Available at: DOI:10.1115/1.4002883

27. Chaker M., Mee T. Design Consideration of Fogging and Wet Compression Systems as Function of Gas Turbine Inlet Duct Configurations. ASME Turbo Expo: Turbine technical conference and exposition GT2015. 2018. pp. 1–14.

28. Chaker M A. Key Parameters for the Performance of Impaction-Pin Nozzles Used in Inlet Fogging of Gas Turbine Engines. Journal of Engineering for Gas Turbines and Power. 2007; 129(2): 473. Available at: DOI:10.1115/1.2364006

29. Savic S., Mitsis G., Haertel C., Khaidarov S., Pfeiffer P. Spray Interaction and Droplet Coalescence in Turbulent Air-Flow. Experimental Study With Application To Gas Turbine High Fogging. 2002; (September): 40–45.

30. Chaker M A. Key Parameters for the Performance of Impaction-Pin Nozzles Used in Inlet Fogging of Gas Turbine Engines. Journal of Engineering for Gas Turbines and Power. 2007; 129(2): 473. Available at: DOI:10.1115/1.2364006

31. Malvern Instruments Ltd. man0368 Issue 3.0. Spraytec User Manual. Worcestershire; 2007.

32. ASME. Gas Turbine Inlet Air-Conditioning Equipment- Appendix A Method of Testing Atomizing Nozzles PTC 51 - 2011. 1st edn. 2011. 132 p.

33. Chaker M., Meher-Homji CB., Mee T. Inlet Fogging of Gas Turbine Engines—Part II: Fog Droplet Sizing Analysis, Nozzle Types, Measurement, and Testing. Journal of Engineering for Gas Turbines and Power. 2004; 126(3): 559. Available at: DOI:10.1115/1.1712982

34. Chaker M., Meher-homji CB., MEE TI. Inlet Fogging of Gas Turbine Engines- Experimental and Analytical Investigations on Impaction Pin Fog Nozzle Behaviour GT-38801. ASME Turbo Expo 2003: Power for Land Sea and Air. Atlanta; 2003. pp. 1–17.

35. Bhargava RK., Meher-Homji CB., Chaker M a., Bianchi M., Melino F., Peretto A., et al. Gas Turbine Fogging Technology : A State-of-the-Art Review — Part II : Overspray Fogging — Analytical. Journal of Engineering for Gas Turbines and Power. 2007; 129(April 2007). Available at: DOI:10.1115/1.2364004

36. Chaker M., Meher-Homji CB. Gas Turbine Power Augmentation: Parametric Study Relating to Fog Droplet Size and Its Influence on Evaporative Efficiency. Journal of Engineering for Gas Turbines and Power. 2011; 133(9): 092001. Available at: DOI:10.1115/1.4002883

37. Chaker M., Meher-Homji CB., Mee T. Inlet Fogging of Gas Turbine Engines—Part II: Fog Droplet Sizing Analysis, Nozzle Types, Measurement, and Testing. Journal of Engineering for Gas Turbines and Power. 2004; 126(3): 559. Available at: DOI:10.1115/1.1712982

38. Daly M. Jane's Aero-engines. 2nd edn. IHS (ed.) Janes Information Group; 2015. 449 p.

39. Volponi AJ. Gas Turbine Parameter Corrections. Journal of Engineering for Gas Turbines and Power. 1999; 121(October 1999): 613–621.

40. Turbomecha. Turbomeca Artouste 520 Airborne Auxiliary Power Trident Installation Manual.

1971.

41. Igie U., Diez-Gonzalez P., Giraud A., Minervino O. Evaluating Gas Turbine Performance Using Machine-Generated Data: Quantifying Degradation and Impacts of Compressor Washing. Journal of Engineering for Gas Turbines and Power. 2016; 138(12): 122601. Available at: DOI:10.1115/1.4033748

42. ICAO-International Civil Aviation Organisation. Environmental Protection, Annex 16, Volume II Aircraft Engine Emissions. Chicago; 2008.

43. Spalding DB. Combustion and Mass Transfer. 1st edn. London: Pergamon Press; 1979. 406 p.

44. Zheng Q., Sun Y., Li S., Wang Y. Thermodynamic Analyses of Wet Compression Process in the Compressor of Gas Turbine. Journal of Turbomachinery. 2003; 125(3): 489. Available at: DOI:10.1115/1.1575254

45. Hill PG. Aerodynamic and Thermodynamic Effects of Coolant Injection on Axial Compressors. The Aeronautical Quarterly. 1963; November: 331–348.

46. Bhargava R., Meher-Homji CB. Parametric Analysis of Existing Gas Turbines With Inlet Evaporative and Overspray Fogging. Volume 4: Turbo Expo 2002, Parts A and B. 2002; 4 A(January 2005): 387–401. Available at: DOI:10.1115/GT2002-30560

47. Wilcox EC., Trout AM. Analysis of Thrust Augmentation of Turbojet Engines by Water Injection at Compressor Inlet Including Charts for calculation Compression Process with Water Injection. 1951.

48. Sanaye S., Tahani M. Analysis of gas turbine operating parameters with inlet fogging and wet compression processes. Applied Thermal Engineering. Elsevier Ltd; 2010; 30(2–3): 234–244. Available at: DOI:10.1016/j.applthermaleng.2009.08.011

49. Roumeliotis I., Mathioudakis K. Evaluation of water injection effect on compressor and engine performance and operability. 2010; 87: 1207–1216. Available at: DOI:10.1016/j.apenergy.2009.04.039

50. Lefebvre AH., Dilip RB. Gas Turbine Combustion Alternative Fuels and Emissions. 3rd edn. New York: CRC Press; 2010. 560 p.

51. ICAO. ICAO Engine Exhaust Emissions Data Bank. 2013. Available at: https://www.easa.europa.eu/document-library/icao-aircraft-engine-emissions-databank#6

Appendix A- Nozzle Selection

Figure A1 shows the behaviour of the four types of nozzles investigated here when subjected to increasing pressure. The Flat Spray (FS) nozzles are rated at low pressures and can produce droplets in the range of 100 – 450 micron at the highest tested pressure of 90 bar. The hollow cone nozzles (HC), despite having different spraying angles, all had very similar droplet diameters throughout the pressure range investigated. The droplet sizes were also too large for the required application. The Impaction pin (IP) and Swirl Jet Nozzles (SJ) produced the smallest diameters of all, and operate at higher pressure ranges. An IP nozzle was selected over the SJ as they are capable of delivering the higher flow-rate required to meet the targeted 2% water-to-air ratio.

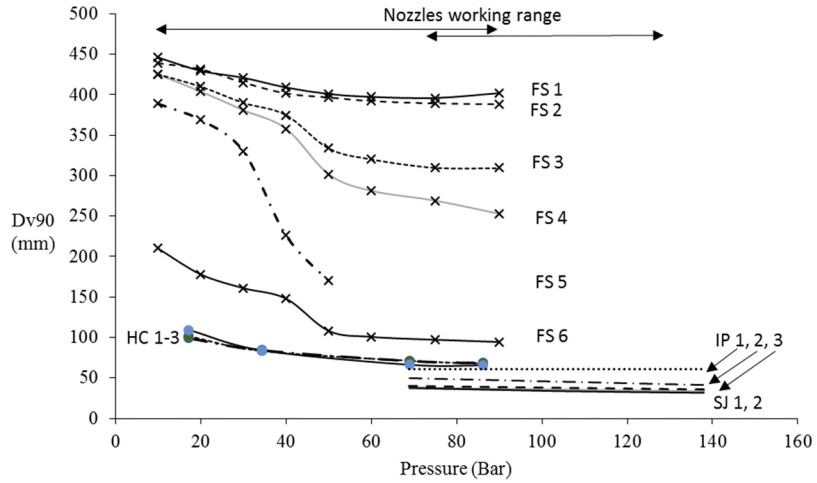

Figure A 1 Behaviour of droplet size (Dv90) for 11 different nozzles at increasing pressure.

Appendix B- Statistical significance of the data

Droplet measurement:

The values reported on the main text for droplet size are time-averages of the readings taken from the laser. The laser software has a function that allows the user to select a time range, in our case being 1- 2 minutes (60- 120 readings), and to get a time-averaged size of the droplet distribution for that range. Figure B1 shows the droplet diameter with time for the case when the water was applied to moving flow (engine intake). It can be seen that despite the fact that the readings were taken for 2 minutes, the droplet size values are quite stable. This was the case for most of the reported values on the main text.

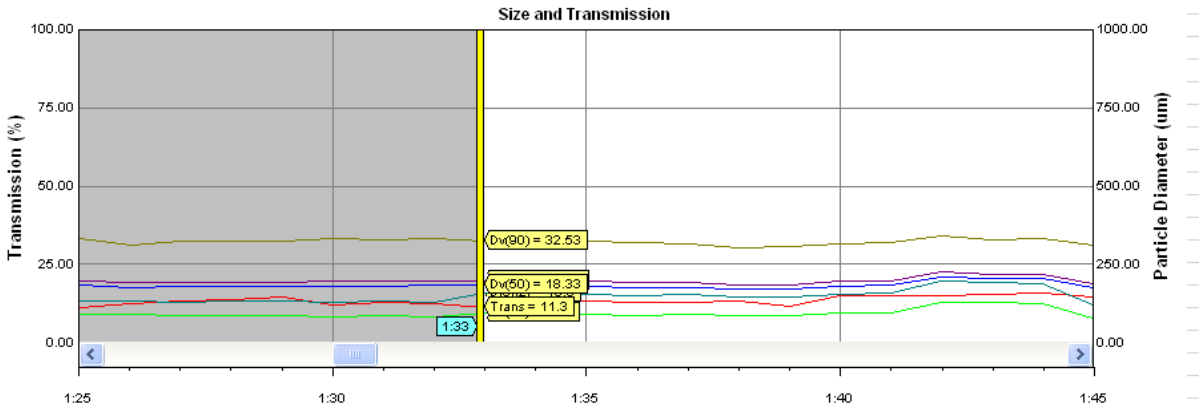

Figure B 1 Droplet Size Distribution with time

Engine Performance Monitoring

The values presented on Figs 10, 11 and Tab.2 are the result of time-averaging each performance parameter, and comparing it to its corresponding dry case. For example, the "dry" CDT was monitored for 8 minutes, and about 480 readings were taken. Water was then injected and the CDT was monitored for another 8 minutes. The average and standard deviation of each sample, for each performance parameter were recorded. Then, a normal probability distribution curve was fitted to the results following Eq. B1.

Where σ is the standard deviation, x is each individual temperature (or pressure) reading, and μ is the mean of all the measurements.

$$P(x) = \frac{1}{\sigma\sqrt{2\pi}} e^{-\frac{(x-\mu)^2}{2\sigma^2}} \quad \text{(B1)}$$

The probabilistic distribution for the CDT when water was injected at a ratio of 2% is shown in Fig, B2-Left. In this case, the mean of the 480 readings was 436.11 K and the Standard deviation 0.467 K (0.11%). For this case, and all the others observed, even if a confidence level of 2 standard deviations (2σ) is taken (95.4% confidence), the mean won't change significantly since the SD is so low.

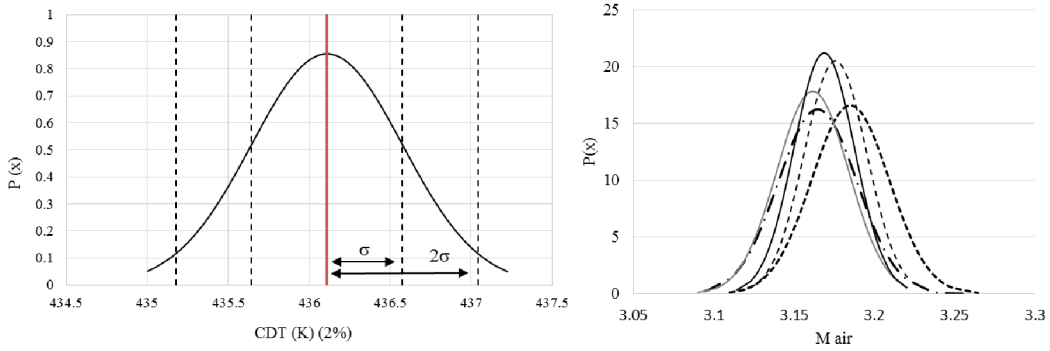

Figure B 2 Normal distribution of the means of CDT (2%) (Left, and Air mass flow (dry)(Right)

Figure B2-Right shows a similar distribution but this time for the air mass flow (dry) and comparing 5 experiments. Each Gaussian curve represents one case. It can be noted that the mean values of each curve are very close together. The distance between these means can be evaluated by the Standard Deviation between the experiments. A similar SD is presented in Tab.2 comparing the changes in performance with water injection for different experiments, against their corresponding dry value. Figure B2- Left represents the case for 2%, and it can be plotted alongside the cases for 1%, 0.5% and dry as seen in Figure B3. The temperature is seen to reduce with increasing injection ratio, but also it is also perceivable how close the distributions are from the mean. This all is an indicator that the averaged values used for the analysis are representative of the conditions of the gas inside the engine, and the experiments have good repeatability.

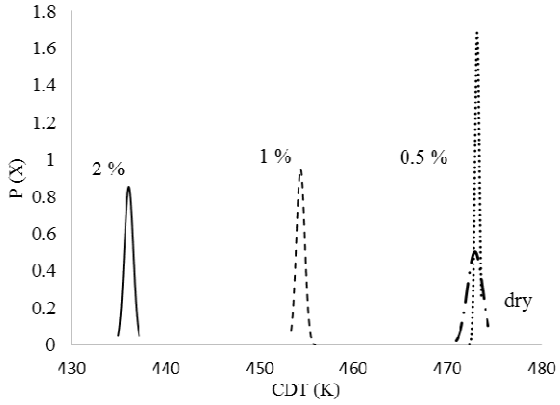

Figure B 3 Normal distribution of CDT for the case of dry, and 0.5-2% injection ratio

Cranfield University

CERES Research Repository **https://dspace.lib.cranfield.ac.uk/**

School of Aerospace, Transport and Manufacturing (SATM) Staff publications (SATM)

Experimental investigation of gas turbine compressor water injection for NOx emission reductions

Block novelo, David alejandro

2019-04-03

Attribution-NonCommercial-NoDerivatives 4.0 International

Block Novelo DA, Igie U, Prakash V, Szymanski A. (2019) Experimental investigation of gas turbine compressor water injection for NOx emission reductions, Energy, Volume 176, June 2019, pp. 235-248

https://doi.org/10.1016/j.energy.2019.03.187

Downloaded from CERES Research Repository, Cranfield University